IEEE Photonics Journal
An IEEE Photonics Society Publication

Open Access

Novel Compact and Low-Cost Ultraweak Fabry–Perot Interferometer as a Highly Sensitive Refractive Index Sensor

Volume 9, Number 5, October 2017

Pengcheng Chen
Xuewen Shu
Haoran Cao

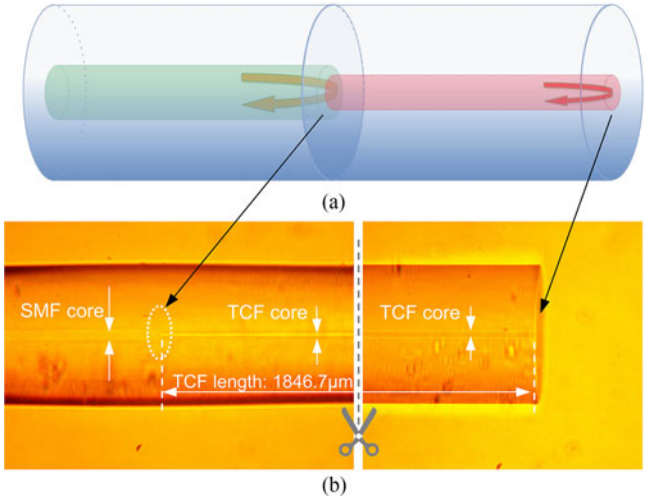

DOI: 10.1109/JPHOT.2017.2732957
1943-0655 © 2017 IEEE

Novel Compact and Low-Cost Ultraweak Fabry–Perot Interferometer as a Highly Sensitive Refractive Index Sensor

Pengcheng Chen, Xuewen Shu, and Haoran Cao

Wuhan National Laboratory for Optoelectronics & School of Optical and Electronic Information, Huazhong University of Science and Technology, Wuhan 430074, China

DOI:10.1109/JPHOT.2017.2732957

Manuscript received May 23, 2017; revised July 16, 2017; accepted July 24, 2017. Date of publication July 28, 2017; date of current version October 11, 2017. This work was supported in part by the Director Fund of WNLO, in part by the National 1000 Young Talents Program, China, and in part by 111 Project (No. B07038). Corresponding author: Xuewen Shu (e-mail: xshu@hust.edu.cn).

Abstract: A novel compact refractive index (RI) sensor based on an ultra-weak intrinsic fiber Fabry-Perot interferometer (FPI) is proposed and demonstrated, which is simply fabricated by splicing a tiny section of thin-core fiber to a single-mode fiber. Such an FPI exhibits an average RI sensitivity of 240dB/RIU over a wide RI range of 1.3326–1.4305, with a maximum sensitivity of 1110.7dB/RIU at the RI of 1.4305. In addition, the FPI can also achieve the simultaneous measurement of the RI and temperature.

Index Terms: Optical fiber, refractive index sensing, Fabry-Perot interference, high sensitivity, fiber fusion, no temperature crosstalk.

1. Introduction

Compared with traditional refractometers, such as Abbe refractometers, all optical fiber-based refractive index (RI) sensors have received much attention recently due to their inherent advantages of simple structure, small size, low cost and suitable for remote sensing. Various fiber-based RI sensors, including fiber Bragg gratings (FBG) [1], long period fiber gratings (LPG) [2], fiber surface plasmon resonance (SPR) [3], and a variety of interferometers [4]–[13], etc., have been widely studied. However, most of the reported fiber RI sensors are wavelength-modulated sensors, which usually have temperature cross-talk and require expensive wavelength demodulation instruments although some of them can achieve high RI sensitivity or resolution (for example, 3.55×10^{-6} reported in [12] with OSA resolution of 1 pm).

To date, fiber-based intensity-modulated refractometers have also been proposed to measure RI, including microholes [14], multimode interferometers (MMI) [15], Michelson interferometers (MI) [16], [17] and Fabry-Perot interferometers (FPI) [18]–[27]. Among these schemes, the FPI based sensor is outstanding due to its ability to measure the RI and temperature simultaneously by demodulating the intensity variation (or contrast) of the interference fringes together with the wavelength shift of the interference spectrum. Thus, the cross-talk between the RI and temperature can be eliminated by simultaneous intensity and phase demodulation. Unfortunately, the sensitivities or resolutions of those reported intensity-modulated RI are relative low (6.7×10^{-5} [14], 3.8×10^{-4}

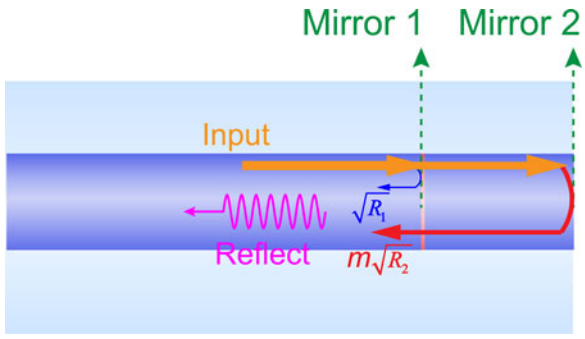

Fig. 1. Illustration of the low fringe contrast intrinsic FPI model.

[15], 1×10^{-3} [18], 6.2×10^{-5} [19], 4.2×10^{-5} [20], 2×10^{-5} [21], 3.4×10^{-5} [22], 1.4×10^{-5} [24], 1.7×10^{-5} RIU [26] and 1.5×10^{-5} [27]), which greatly limits them in the practical applications.

Recently, by introducing a refractive index-modified dot (RIMD) in single mode fiber (SMF) with a femtosecond laser, we have developed a low fringe contrast FPI and also revealed that there are two ultra-sensitive zones existing in such FPI based RI sensors [28]. The fabrication process for the RIMD is straightforward while the device is compact, robust and assembly-free. However, the micromachining method needs expensive computer-controlled translation stage system and femtosecond laser, which is an important factor that needs to be considered in some practical applications.

Thin-core fiber (TCF) has been widely used for fabricating transmissive and reflective modal interferometers such as MMI [29], [30] and MI [16], [17]. As for a transmissive MMI, the size of the device is usually large. An MI is a reflective probe, but its size is still not small enough. To obtain a high fringe contrast interference spectrum, lateral offset splicing [16] or additional reflective surface [17] are required, which increases the manufacture steps and costs. Compared with MMIs and MIs, FPIs are far more compact and simple in structure.

In this paper, we demonstrate a highly sensitive intensity-modulated RI sensor based on a compact and ultra-weak in-line FPI, which was fabricated by splicing a tiny section of TCF to a lead standard SMF. Due to the slightly differential refractive index between the cores of the two fibers, a low fringe contrast FPI is obtained in air, while high fringe contrast can be obtained in solutions, especially when the surrounding RI is near the ultra-sensitive zones. The fabricated sensor exhibits a high average RI sensitivity of 240 dB/RIU over a wide RI range of 1.3326–1.4305, with a maximum sensitivity up to 1110.7 dB/RIU and a resolution of 9×10^{-7} RIU at the RI of 1.4305, which is near the ultra-sensitive zone. Compared with other intensity-modulated RI sensors based on fiber fusion splicing technique, the sensitivity of our device is generally one order of magnitude higher [15]–[17]. Moreover, the RI sensor also exhibits the ability to measure the surrounding refractive index (SRI) and temperature simultaneously, with a temperature sensitivity of 10.1 pm/°C. The proposed device possesses the advantages of compact size, easy fabrication, low cost, high sensitivity and no temperature cross-talk.

2. Basic Principle

The basic structure of our proposed intrinsic FPI is illustrated in Fig. 1. There are two reflection mirrors in the sensor head: Mirror 1 (within the fiber) and Mirror 2 (at fiber end) with reflection coefficients of R_1 and R_2, respectively. Here, $R_2 = [(n_{co} - n_{SRI})/(n_{co} + n_{SRI})]^2$, with n_{co} and n_{SRI} being the index of the fiber core and SRI, respectively. Thus the normalized strength of the interference

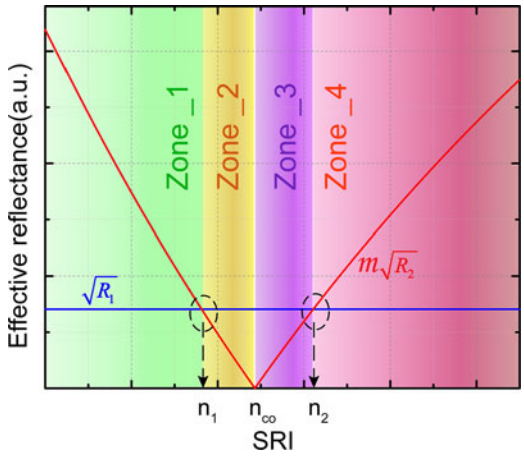

Fig. 2. Variation of the effective reflectance with the SRI.

fringes can be modeled using the following equation:

$$I = R_1 + m^2 R_2 + 2\sqrt{R_1 R_2} m \cos(2\varphi) \quad (n_{ex} \le n_{co})$$
$$I = R_1 + m^2 R_2 - 2\sqrt{R_1 R_2} m \cos(2\varphi) \quad (n_{ex} > n_{co}) \tag{1}$$

Where $m = (1-\alpha)(1-\gamma)(1-R_1)$, $\varphi = 4\pi n_{co} L/\lambda$ is the phase shift in the cavity, L is the length of the cavity; α is the intensity attenuation factors of the Mirror 1; γ is defined as the transmission loss factor of the cavity.

From Eq. (1), the interference fringe visibility V can be derived as:

$$V = \frac{I_{\max} - I_{\min}}{I_{\max} + I_{\min}} = \frac{2\frac{m\sqrt{R_2}}{\sqrt{R_1}}}{1 + \left(\frac{m\sqrt{R_2}}{\sqrt{R_1}}\right)^2} \tag{2}$$

As the Mirror 1 is located in the fiber core completely, the SRI has no influence on the R_1, i.e., the value ofR_1 is a constant in RI measurement, and one can see that only R_2 depends on the SRI to be measured. Therefore the effective reflection coefficient of Mirror 1 and 2 can be explained as:

$$\sqrt{R_1} = const$$
$$m\sqrt{R_2} = m\left|\frac{n_{co} - n_{SRI}}{n_{co} + n_{SRI}}\right| \tag{3}$$

Here, we assume that the $\sqrt{R_1} \ll m\sqrt{R_2}$ in the air ($n_{SRI} = 1$). Thus $V \sim 0$, i.e., the visibility of the interference fringe pattern is very low in the air. However, when the SRI is increased within a certain range, the value of $m\sqrt{R_2}$ will decrease and will approach $\sqrt{R_1}$, V will increase to ~1, which means maximum visibility can be obtained. As a result, the dip intensity of the wavelength or the contrast of the interference fringe variation against the SRI variation will be observed.

Fig. 2 shows the relationship between the $\sqrt{R_1}$ (constant) and $m\sqrt{R_2}$(changing with the SRI) versus SRI, respectively. It is obvious that there are two crossing points (n_1 and n_2) between the straight line ($\sqrt{R_1}$) and the curved line ($m\sqrt{R_2}$), and four different zones can be divided (i.e.,$n < n_1$, $n_1 < n < n_{co}$, $n_{co} < n < n_2$ and $n > n_2$, marked as zone_1-4, respectively), which have different response trends for SRI sensing.

In order to illustrate this visually, we can simulate the evolution of the reflection spectra of the RI sensor versus the SRI according to Eq. (1), as shown in Fig. 3(a)–(d). Note that the specific experimental parameters are unknown, the parameters used in the simulation are assumed to be: m = 0.226, $n_{co} = 1.47$, $\sqrt{R_1} = 0.0034$, L = 50 μm. These assumptions have no effect on

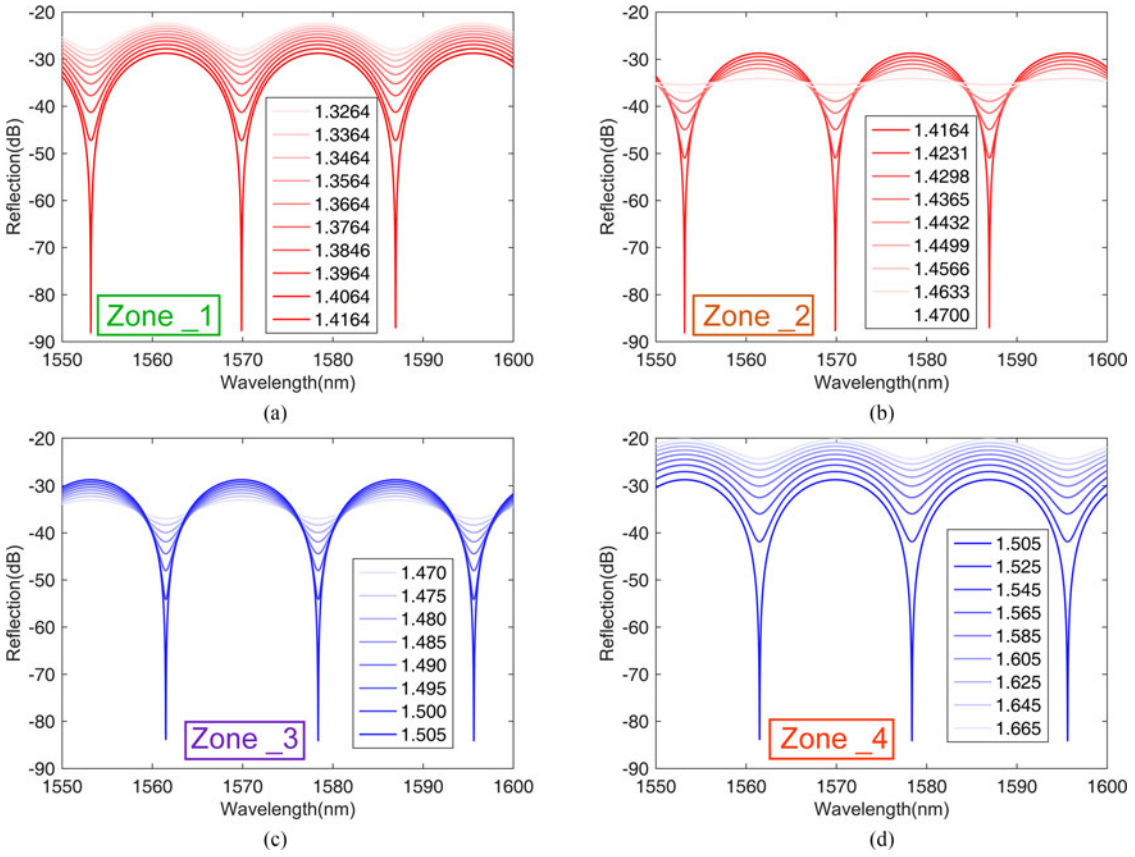

Fig. 3. (a)–(d) Simulated reflective spectra of FPI in four RI regions, respectively.

our understanding of the intrinsic phenomenon because the trend is consistent. It can be seen in Fig. 3(a)–(d) that the dip strength of the fringe change quickly as the SRI approaches the transition regions between zone_1 and 2 and zone_3 and 4 respectively. The rate of change reaches maximum when the SRI values around n_1 and n_2 shown as the intercept points in Fig. 2. It is evident that there are two extremely sensitive zones (RI near n_1 and n_2), where the RI sensitivity exhibits a flip-flop feature and reaches an ultra-high sensitivity for RI sensing. And there is a π-phase shift between the cases of RI $< n_{co}$ and RI $> n_{co}$ due to the half-wave loss. Moreover, according to Eq. (3), when $\sqrt{R_1} = m\sqrt{R_2}$, one can calculate the values of the two crossing points, which are found to be $n_1 = 1.4164$ and $n_2 = 1.5049$. And from Fig. 3(a)–(d), one can see clearly that the values of the two crossing points are $\sim$1.4164 and 1.505, respectively, which means that the evolution of the reflection spectra of the sensor versus the SRI (see Fig. 3) is agree well with the effective reflectance model (see Fig. 2).

3. Device Fabrication

The schematic of our proposed RI sensor based on FPI is shown in Fig. 4(a). The fabrication process of the differential mirror reflectance FPI only involved fiber cleaving and fusion splicing. The specific processes were as follow: first, a section of end cleaved single mode Erbium-Ytterbium co-doped TCF (DF1500Y) with core and cladding diameter of $\sim$5 μm and 125 μm, respectively, was spliced to a standard communication SMF (YOFC.) by a commercial fusion splicer (FEM-80S, Fujikura) in the automatic mode, to form mirror 1 at the SMF/TCF fusion interface. Then the other end of the TCF was cleaved with a certain length to obtain Mirror 2. A broadband source (BBS), an optical spectrum analyzer (OSA, AQ6370, Yokogawa) and a fiber circulator were used to monitor

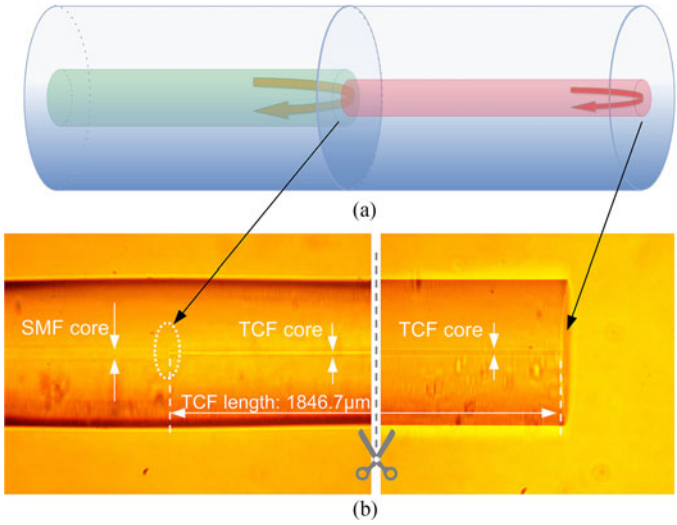

Fig. 4. (a) Schematic of the fabricated FPI. (b) Microscope image of the FPI near the splicing point at the SMF/TCF interface and near the end face of the TCF.

the interference spectrum. Fig. 4(b) shows the microscope image of the FPI fabricated in the fiber, where the measured TCF length is ∼1846.7 μm.

The normalized reflection spectrum of one sample is shown in Fig. 5(a), where it is clearly seen that, a low fringe contrast interference spectrum is obtained in air. The fringe visibility is only ∼1.2 dB and the free spectral range (FSR) is ∼0.4 nm. Note that the normalized reflectance spectrum intensity in the air is greater than 0, which indicates that after the sensor was fabricated, compared with the reflectivity of the original SMF end face, the total reflectivity of the reflectors increases. The FPI end face Fresnel reflection mainly comes from the TCF/air interface, while the original SMF end face Fresnel reflection comes from the SMF/air interface, which means that the reflectivity of the TCF/air interface is larger than the SMF/air interface. The DF1500Y single mode optical fiber has exceptionally high doped concentration, which makes the index of the DF1500Y TCF core slightly larger than the YOFC SMF core. Therefore, the normalized reflectance spectrum intensity in the air is greater than 0.

4. Refractive Index Test and Discussion

To verify the ultra-sensitivity zone indicated in theoretical analysis, we examined the FPI tip at SRI with different concentrations of sucrose solutions. The RI of the sucrose solutions were calibrated by an Abbe refractometer at room temperature. After each measurement, the sensor head was carefully cleaned with alcohol to eliminate the residual test liquid on the end face of the fiber until its original spectrum is recovered in the air for next RI test. As shown in Fig. 5(a), the intensity of the reflection spectrum decreases gradually when the RI increases from 1.0000 (air), 1.3326 (water) to 1.4305 (sucrose solution) and the visibility of the interference fringes increases gradually at the same time. The initial visibility is only ∼1.2 dB when the device is in the air. When the probe is in the liquid (1.3326 $<$ RI $<$ 1.4305), the visibility increases with the RI increasing and it reaches ∼22 dB at the RI of 1.4305. However, when the RI increases from 1.4305 to 1.4639, the visibility decreases gradually, as shown in Fig. 5(b). And when the RI continues to increase from 1.4731 to 1.4963, the reflection spectrum variation trend is similar to the RI range (1.3326 to 1.4305), as shown in Fig. 5(c). Fig. 5(d) shows the relationship of the strength of the deepest dip (∼1500.56 nm for RI $< n_{co}$ and 1500.36 nm for RI $> n_{co}$, respectively) versus the SRI. It is evident that there is an extremely sensitive zone near the RI of 1.4305, where the RI sensitivity exhibits a flip-flop feature and reaches an ultra-high sensitivity for RI sensing. More interesting, as shown in

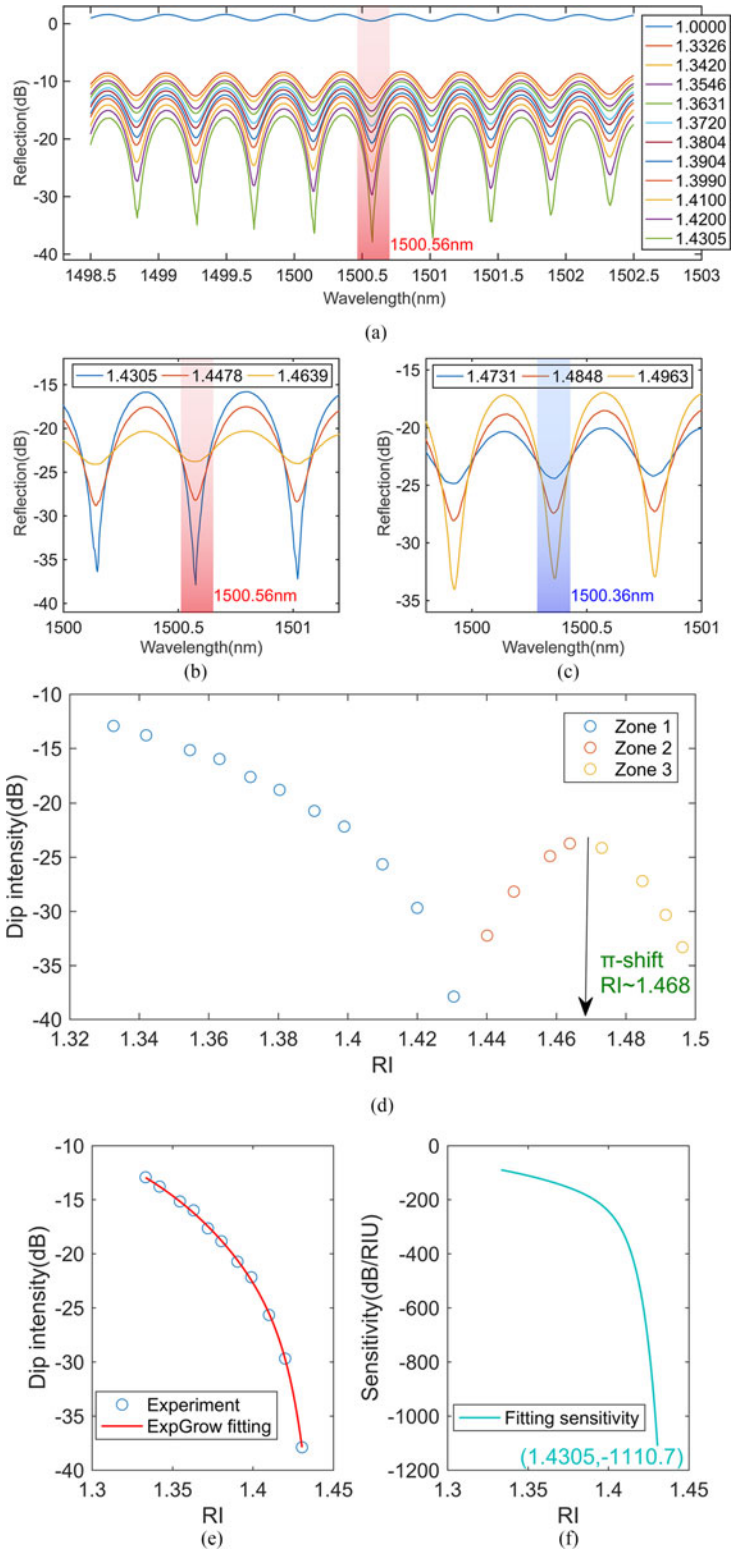

Fig. 5. (a)–(c) Measured reflective spectra of FPI in zone_1-3, respectively. (d) Measured fringe dip intensity at 1500.56 nm and 1500.36 nm in regions versus RI in zone_1-3, respectively. (e) Measured fringe dip intensity at 1500.56 nm versus SRI and its rational fitting curve in zone_1. (f) Measured RI sensitivity in zone_1.

TABLE 1
Sensitivity of Various Intensity-Modulated Fiber RI Sensors Based on Splicing Fusion

Sensor types	Key structure	Maximum sensitivity/(dB/RIU)
MMI [12]	SMF-MMF	110
MI [13]	SMF- lateral TCF	202
MI [14]	SMF-TCF-SMF	208
FPI [16]	SMF-HCF	16
FPI [17]	SMF-laser drilling hole	37
FPI [19]	SMF-HF etching hole	29.7
FPI [20]	SMF-Au film-SMF	43.6
FPI [21]	SMF-fiber film-SMF	72.6
FPI [23]	SMF-PCF	21.5
This paper	SMF-TCF	1110.7

Fig. 5(d), we can estimate the index of the DF1500Y fiber core is ∼1.468, which corresponds to the π-phase shift point. The π-phase shift occurs since the light is reflected from an interface from an optically thinner medium to an optically denser medium when the SRI $>$ 1.468. Therefore, by using $L_{cavity} = \lambda^2/2n_{co}FSR$, we can calculate the TCF fiber length, i.e., the cavity length, to be ∼1916.8 μm, which is close to the measured value (∼1846.7 nm). Further more, by combining the value of TCF core index and the equation: $(n_{co} - n_1)/(n_{co} + n_1) = (n_2 - n_{co})/(n_2 + n_{co})$, where $n_1 = 1.4305$, $n_{co} = 1.468$, one can calculate the value of the second RI extremely sensitive zone (n_2) to be ∼1.5065, which is beyond the maximum refractive index of the test sucrose solutions. We would also point out here that one may also use the fringe contrast as an indicator to measure RI since the fringe contrast has a similar variation trend when RI changes. Fig. 5(e) shows the relationship between the strength of the 1500.56 nm dip and the SRI for experimental measurement. The dip intensity of the interference fringe decreases rapidly with the increase of the SRI. The fitting curve is adopted in rational fitting, with a correlation coefficient (R^2) of 0.9996 for the experimental data, as shown in Fig. 5(e). It is clearly seen that the trend of the response of the dip strength to the SRI in the experiment is similar to the simulation shown in Fig. 2. Fig. 5(f) shows the derivative of the fitted equation, the sensitivity of the fringe dip intensity to the SRI is found to be ∼1110.7 dB/RIU at the RI of 1.4305, and with an average RI sensitivity of 240 dB/RIU over a wide RI range of 1.3326-1.4305. The measurement resolution for the SRI, $\delta(RI)$, can be calculated by $\delta(RI) = \delta P/S$, where δP is the power resolution of the OSA and S is the RI sensitivity. Given $\delta P = 0.001$ dB and $S = 1110.7$ dB/RIU, a high RI resolution of 9.0×10^{-7} RIU could be achieved at the RI of 1.4305, which is much higher than the reported other intensity modulated RI sensors based on fiber splicing technology, as shown in Table 1.

Note that there is fiber core mismatch between the SMF and the TCF, so a sparse envelop modulation may come from a Michelson interference, which is caused by the end face of the TCF cladding and TCF core. Since the period of the MI spectrum is much larger than the FPI, we ignore the influence of the MI and only consider the FPI in our experiments.

In order to analyze the number and the power distribution of the reflection interference light, a fast Fourier transform (FFT) is taken to obtain the spatial frequency, as shown in Fig. 6. As we can see, there is one main peak (2.3 nm^{-1}) in the spatial frequency spectrum, which corresponds to the thin core fiber cavity. One weak peak (2 nm^{-1}) on the left side of the main peak corresponds to the TCF cladding cavity; and other weak peaks (integer multiples of the main cavity) on the right side of the main peak are corresponding the secondary and multiple reflections of TCF core cavity.

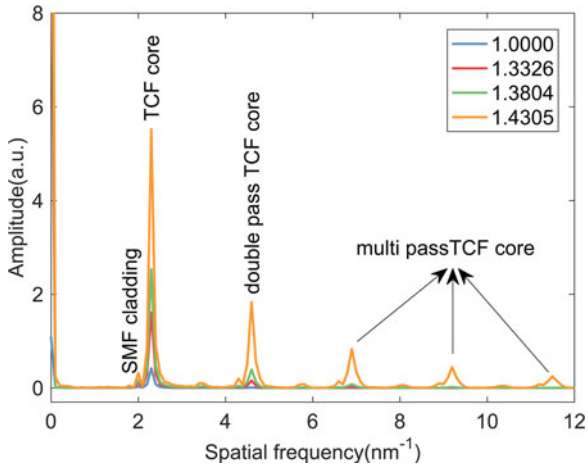

Fig. 6. Measured spatial frequency spectra at different SRI.

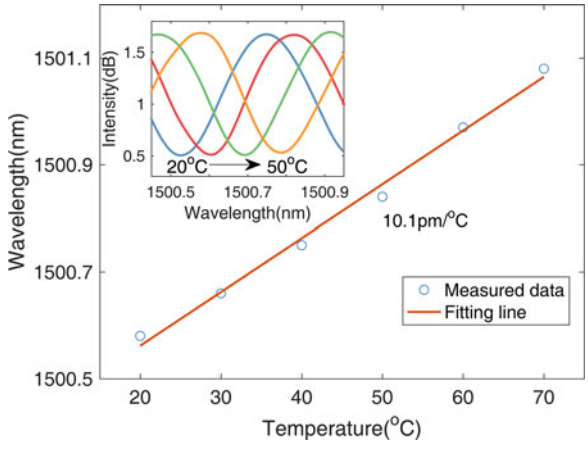

Fig. 7. Temperature response of the dip wavelength. Insert: interference spectra under different temperature.

As the diameter of the SMF core is bigger than the TCF, when light goes through the fusion point of the fiber, most of the power will transmit into the TCF core, which acts as the primary cavity. A small portion of the optical power will transmit into the TCF cladding, which acts as a weak cavity. With the SRI increasing from 1.000 to 1.4305, the intensity of all these spatial frequency peaks also increase.

5. Temperature Response

The temperature response of the sensors was also characterized. The sensor head was placed onto a heater with temperature increasing from 20 °C to 70 °C. As shown in the insert of Fig. 7, the dip wavelength of reflection interference has an obvious horizontally red shift with the increasing temperature and a linear function is adopted to fitting the wavelength-temperature response with a sensitivity of 10.1 pm/°C. It is noteworthy that the intensity of the spectrum is nearly unchanged, which means that our sensors can achieve the simultaneous measurement of SRI and temperature by monitoring the intensity of the resonance dip and the wavelength of the resonance respectively and thus solve the cross-sensitivity problem between temperature and SRI. As the RI of a liquid is usually temperature dependent, the simultaneous measurement is extremely advantageous [31].

6. Conclusions

In conclusion, a simple, easy to fabricate, compact and low cost FPI is proposed, which is formed by fusing a tiny section of TCF to SMF. Due to the small differential refractive index between the cores of the two fibers, a low fringe contrast ultra-weak intrinsic FPI is obtained in air. For such simple FPI, our investigation also confirms the existing of two ultra-sensitive zones for RI sensing. The measured SRI sensitivity is up to ∼1110.7 dB/RIU at the SRI of 1.4305, which is obviously much higher than those reported intensity-modulated RI sensors based on fiber splicing technology. Moreover, the structure can also be used to monitor temperature with a sensitivity of 10.1 pm/°C, which indicates that it has the capability to measure the SRI and temperature simultaneously. The combination of high sensitivity, simple-structure and the ability to overcome the temperature cross sensitivity problem could make it promising in the field of bio-chemical sensing applications.

References

[1] N. Chen, B. Yun, and Y. Cui, "Cladding mode resonances of etch-eroded fiber Bragg grating for ambient refractive index sensing," *Appl. Phys. Lett.*, vol. 88, no. 13, 2006, Art. no. 133902.

[2] H. J. Patrick, A. D. Kersey, and F. Bucholtz, "Analysis of the response of long period fiber gratings to external index of refraction," *J. Lightw. Technol.*, vol. 16, no. 9, pp. 1606–1612, Sep. 1998.

[3] P. Bhatia and B. D. Gupta, "Surface-plasmon-resonance-based fiber-optic refractive index sensor: sensitivity enhancement," *Appl. Opt.*, vol. 50, no. 14, pp. 2032–2036, May 2011.

[4] L. Xu, Y. Li, and B. Li, "Nonadiabatic fiber taper-based Mach-Zehnder interferometer for refractive index sensing," *Appl. Phys. Lett.*, vol. 101, no. 15, 2012, Art. no. 153510.

[5] C. Wu, Z. Liu, A. P. Zhang, B. O. Guan, and H. Y. Tam, "In-line open-cavity Fabry-Perot interferometer formed by C-shaped fiber fortemperature-insensitive refractive index sensing," *Opt. Exp.*, vol. 22, no. 18, pp. 21757–21766, Sep. 2014.

[6] Q. Wang and G. Farrell, "All-fiber multimode-interference-based refractometer sensor: Proposal and design," *Opt. Lett.*, vol. 31, no. 3, pp. 317–319, Feb. 2006.

[7] R. Jha, J. Villatoro, G. Badenes, and V. Pruneri, "Refractometry based on a photonic crystal fiber interferometer," *Opt. Lett.*, vol. 34, no. 5, pp. 617–619, Mar. 2009.

[8] W. C. Wong, C. C. Chan, L. H. Chen, Z. Q. Tou, and K. C. Leong, "Highly sensitive miniature photonic crystal fiber refractive index sensor based on mode field excitation," *Opt. Lett.*, vol. 36, no. 9, pp. 1731–1733, May 2011.

[9] K. Milenko *et al.*, "Photonic crystal fiber tip interferometer for refractive index sensing," *Opt. Lett.*, vol. 37, no. 8, pp. 1373–1375, Apr. 2012.

[10] W. Tingting, G. Yixian, C. Jianhua, and W. Ming, "Wavelength-interrogation Fabry–Perot refractive index sensor based on a sealed in-fiber cavity," *IEEE Photon. Technol. Lett.*, vol. 28, no. 1, pp. 3–6, Jan. 2016.

[11] X.-G. Li, Y. Zhao, L. Cai, and Q. Wang, "Simultaneous measurement of RI and temperature based on a composite interferometer," *IEEE Photon. Technol. Lett.*, vol. 28, no. 17, pp. 1839–1842, Sep. 2016.

[12] Y. Zhao, F. Xia, and J. Li, "Sensitivity-enhanced photonic crystal fiber refractive index sensor with two waist-broadened tapers," *J. Lightw. Technol.*, vol. 34, no. 4, pp. 1373–1379, Feb. 2016.

[13] T. Wieduwilt, J. Dellith, F. Talkenberg, H. Bartelt, and M. A. Schmidt, "Reflectivity enhanced refractive index sensor based on a fiber-integrated Fabry-Perot microresonator," *Opt. Exp.*, vol. 22, no. 21, pp. 25333–25346, Oct. 2014.

[14] Y. Wang, D. N. Wang, M. W. Yang, W. Hong, and P. X. Lu, "Refractive index sensor based on a microhole in single-mode fiber created by the use of femtosecond laser micromachining," *Opt. Lett.*, vol. 34, no. 21, pp. 3328–3330, Nov. 2009.

[15] S. Silva, O. Frazão, J. L. Santos, and F. X. Malcata, "A reflective optical fiber refractometer based on multimode interference," *Sens. Actuators B: Chem.*, vol. 161, no. 1, pp. 88–92, 2012.

[16] J. Zhou *et al.*, "Intensity modulated refractive index sensor based on optical fiber Michelson interferometer," *Sens. Actuators B: Chem.*, vol. 208, pp. 315–319, 2015.

[17] Z. Li *et al.*, "Temperature-insensitive refractive index sensor based on in-fiber Michelson interferometer," *Sens. Actuators B: Chem.*, vol. 199, pp. 31–35, 2014.

[18] S. F. O. Silva, "Optical fiber refractometer based on a Fabry-Pérot interferometer," *Opt. Eng.*, vol. 47, no. 5, 2008, Art. no. 054403.

[19] H. Y. Choi, G. Mudhana, K. S. Park, U. C. Paek, and B. H. Lee, "Cross-talk free and ultra-compact fiber optic sensor for simultaneous measurement of temperature and refractive index," *Opt. Exp.*, vol. 18, no. 1, pp. 141–149, Jan. 2010.

[20] Z. L. Ran, Y. J. Rao, W. J. Liu, X. Liao, and K. S. Chiang, "Laser-micromachined Fabry-Perot optical fiber tip sensor for high-resolution temperature-independent measurement of refractive index," *Opt. Exp.*, vol. 16, no. 3, pp. 2252–2263, Feb. 2008.

[21] Y.-J. Rao, M. Deng, D.-W. Duan, and T. Zhu, "In-line fiber Fabry-Perot refractive-index tip sensor based on endlessly photonic crystal fiber," *Sens. Actuators A: Phys.*, vol. 148, no. 1, pp. 33–38, 2008.

[22] Y. Ma *et al.*, "Temperature-independent refractive index measurement based on Fabry-Perot fiber tip sensor modulated by Fresnel reflection," *Chin. Opt. Lett.*, vol. 10, no. 5, May 2012, Art. no. 050603.

[23] C.-L. Lee, J.-M. Hsu, J.-S. Horng, W.-Y. Sung, and C.-M. Li, "Microcavity fiber fabry-pérot interferometer with an embedded golden thin film," *IEEE Photon. Technol. Lett.*, vol. 25, no. 9, pp. 833–836, May 2013.

[24] D. Wu, T. Zhu, G. Y. Wang, J. Y. Fu, X. G. Lin, and G. L. Gou, "Intrinsic fiber-optic Fabry-Perot interferometer based on arc discharge and single-mode fiber," *Appl. Opt.*, vol. 52, no. 12, pp. 2670–2675, Apr. 2013.

[25] X.-Y. Zhang *et al.*, "Miniature end-capped fiber sensor for refractive index and temperature measurement," *IEEE Photon. Technol. Lett.*, vol. 26, no. 1, pp. 7–10, Jan. 2014.
[26] D. Wu, Y. Huang, J.-Y. Fu, and G.-Y. Wang, "Fiber Fabry–Perot tip sensor based on multimode photonic crystal fiber," *Opt. Commun.*, vol. 338, pp. 288–291, 2015.
[27] M. Jiang, Q.-M. Sui, Z.-W. Jin, F.-Y. Zhang, and L. Jia, "Temperature-independent optical fiber Fabry–Perot refractive-index sensor based on hollow-core photonic crystal fiber," *Optik*, vol. 125, no. 13, pp. 3295–3298, 2014.
[28] P. Chen, X. Shu, H. Cao, and K. Sugden, "Ultra-sensitive refractive index sensor based on an extremely simple femtosecond-laser-induced structure," *Opt. Lett.*, vol. 42, no. 6, pp. 1157–1160, Mar. 2017.
[29] B. Gu, M. J. Yin, A. P. Zhang, J. W. Qian, and S. He, "Low-cost high-performance fiber-optic pH sensor based on thin-core fiber modal interferometer," *Opt. Exp.*, vol. 17, no. 25, pp. 22296–22302, Dec. 2009.
[30] J. Wu *et al.*, "Low temperature sensitive intensity-interrogated magnetic field sensor based on modal interference in thin-core fiber and magnetic fluid," *Appl. Phys. Lett.*, vol. 104, no. 25, Jun. 2014, Art. no. 252402.
[31] X. Shu, B.A.L Gwandu, Y. Liu, L. Zhang, and I. Bennion, "Sampled fiber Bragg grating for simultaneous refractive-index and temperature measurement," *Opt. Lett.*, vol. 26, no. 11, pp. 774–776, Jun. 2001.